CATTANEO-CHRISTOV DUAL DIFFUSIVE NON-NEWTONIAN NANOLIQUID FLOW FEATURING NONLINEAR CONVECTION

M. Nasir[1], M. Waqas[2,*], M. S. Kausar[1], O. Anwar Bég[3] and Nurnadiah Zamri[1]

[1]*Faculty of Informatics and Computing, University Sultan Zainal Abidin (Kampus Gong Badak), Kuala Terengganu, Terengganu 21300, Malaysia*

[2]*NUTECH School of Applied Science and Humanities, National University of Technology, Islamabad 44000, Pakistan*

[3]*Multi-Physical Engineering Sciences Group, Mechanical Engineering, Salford University, School of Science, Engineering and Environment (SEE), Manchester, M54WT, UK. Email:* O.A.Beg@salford.ac.uk

*Correspondence: muhammadwaqas@nutech.edu.pk (M. Waqas)

Abstract: A theoretical study is presented of the transport characteristics in double diffusive tangent hyperbolic (non-Newtonian) nanofluid boundary layer flow from a stretching flat surface. The Cattaneo–Christov (non-Fourier and non-Fickian) double diffusion model is deployed in the formulations for energy and species conservation, to determine more precisely temperature and concentration distributions with thermal and solutal relaxation times. Non–linear mixed convection and heat generation/absorption are included. The nanofluid approach combines Brownian motion and thermophoresis. Suitable transformations are deployed to render the nonlinear partial differential system into a system of dimensionless coupled ordinary nonlinear differential equations. The non-dimensional boundary value problem is then solved with the homotopic analysis method (HAM). The distributions of velocity, temperature and concentration of nanoparticles are depicted and investigated for the effects of multiple emerging parameters. Velocity is reduced (and momentum boundary layer thickness elevated) with increasing power–law index and Weissenberg number whereas velocity is elevated (and momentum boundary layer thickness reduced) with increment in mixed convection variable. Temperature is suppressed (and thermal boundary layer thickness depleted) with increasing thermal relaxation variable, heat sink parameter, Prandtl number whereas temperature is enhanced (and thermal boundary layer thickness boosted) with greater heat source parameter, Brownian motion parameter and thermophoresis parameter. Nanoparticle concentration is depleted (and concentration boundary layer thickness reduced) with greater Schmidt number and Brownian motion parameter whereas the opposite effect is induced with greater thermophoresis parameter and solutal relaxation time. Skin friction is strongly reduced with increasing values of nonlinear thermal and concentration convection variables. The simulations are relevant to nano-polymer coating operations.

Keywords: *Cattaneo–Christov double diffusion, nonlinear mixed convection, tangent hyperbolic nanofluid, heat generation/absorption; HAM; nano-polymer coating operations.*

1.   Introduction

In recent decades, non–Newtonian fluids have attracted significant interest owing to growing applications in industrial, chemical, bio-technological and mechanical engineering. Examples of both internal and external flows include food processing [1,2], thermal duct processing [3, 4], bioinspired spacecraft pumps [5], geological energy systems [6], gastric transport [7], electroconductive gel pumping in robotics [8], hemo-rheology of the human circulation [9] and biomedical blood pumps [10]. Another key area of technology in which non-Newtonian flows feature is coating operations which may feature stagnation flows [11] and spin deposition [12]. Non–Newton fluids feature many diverse characteristics including weakly elastic dominated by shear thinning, shear thickening, viscoplasticity (yield stress behaviour), viscoelasticity strongly elastic and dominated by elastic stresses etc. Many models have therefore been developed to simulate non-Newtonian behaviour which deviates significantly from classical viscous flow behaviour (Navier-Stokes equations). These models include the Giesekus viscoelastic model (popular for polymers) [13] and the Ostwald-DeWaele power-law model (for rheological coatings) [14, 15]. Although numerous other models are available such as the PPT model, the Johnson-Segalman model and the Maxwell upper convected model (UCM), an alternative model which provides accurate results for decreasing shear effects (i.e., viscosity reduction with increasing shear force) is the *tangent hyperbolic non-Newtonian model*. This model is also very appropriate for certain categories of polymeric coatings and has therefore received considerable attention in recent years in the context of mathematical modelling. Many investigations have been reported with a variety of multi-physical effects using different numerical and analytical methods to accommodate the strong nonlinearity of tangent-hyperbolic flows. Hayat *et al.* [16] discussed the impact of cross diffusion effects (Soret and Dufour) on hydromagnetic stagnation flow of a tangent hyperbolic fluid from a on a permeable convectively heated extending sheet. They noted that with increasing power-law index and Weissenberg number, there is an elevation in the skin friction whereas Nusselt number is suppressed with Dufour parameter and enhanced with Soret number. They further observed that Sherwood number is enhanced with Dufour number whereas it is reduced with Soret number. Hussain *et al.* [17] investigated viscous heating effects on hydromagnetic tangent hyperbolic fluid boundary layer convection flow. Ibrahim [18] considered wall slip effects on tangent hyperbolic fluid flow in a magnetic field. Recently, Khan *et al.* [19] presented homotopy analytical solutions for entropy generation in chemically reacting mixed

convective tangent hyperbolic nanofluid flow with thermal radiation flux. Further studies deploying the tangent hyperbolic non-Newtonian model include Atif *et al.* [20] (on Falkner-Skan wedge external thermo-solutal boundary layer nanofluid flow), Kebede *et al.* [21] (on viscous heating in time-dependent nanofluid wedge flow), Awais *et al.* [22] (on entropy generation), Ramzan *et al.* [23] (on non-Fourier and non-Fickian bioconvective nanofluid reactive magnetohydrodynamic) and Shafiq *et al*. [24] (on Sakiadis bioconvective nanofluid transport). All these studies confirmed the significant modification in momentum, heat and mass transfer characteristics produced with the tangent-hyperbolic rheology.

Mixed convection is an important process featuring in many applications in industry including materials processing, coating deposition, glass manufacturing etc. It involves both forced and free convection acting simultaneously i. e. where both pressure forces and buoyancy forces interact. Fluid density reduces as the fluid temperature increases, which triggers buoyancy effects that arise in natural convection and also mixed convection regimes. Some interesting studies in non-Newtonian mixed convection have been reported and include Metri *et al.* [25] (on viscoelastic stretching sheet mixed convection flow), Çolak *et al.* [26] (on enclosure mixed convection magnetohydrodynamic flow) and Bhukta *et al.* [27] (on dissipative thermoconvective hydromagnetic stretching sheet flow in a porous medium).

The studies described above have generally considered Fourier heat conduction and Fickian mass diffusion. However, in a number of engineering systems, these models are inadequate since thermal relaxation and solutal relaxation effects arise. These necessitate the inclusion of *non-Fourier and non-Fickian models* which can more precisely characterize heat and mass transfer phenomena. The Foruier model predicts infinite thermal wave speeds which are corrected in the Cattaneo [28] formulation. Christov [29] further refined the Cattaneo model, to confirm finite–speed heat conduction. Subsequently a number of researchers have deployed the Cattaneo-Christov model in a variety of both Newtonian and non-Newtonian problems. The Cattaneo–Christov model was implemented for thermal convection of Newtonian fluids by Straughan [30]. Hayat *et al.* [31] investigated the Cattaneo–Christov double–diffusion in Walters' B viscoelastic nanofluid with chemical reaction. Zhang *et al.* [32] computed the transient reactive dissipative flow of Oldroyd-B fluids with Cattaneo-Christov double diffusion. Ahmad *et al.* [33] examined the nanofluid boundary layer flow from a bi-axial stretching sheet with Cattaneo-Christov double diffusion, observing that both temperature and concentration are decreased with non-Fourier

thermal relaxation and non-Fickian solutal relaxation parameters, for the case of prescribed heat flux at the boundary. Ijaz and Ayub [34] used a homotopy method to analyze the reactive dual stratified viscoelastic nanofluid flow from a porous stretching surface with Cattaneo-Christov double diffusion. They noted that temperature is suppressed with increasing thermal relaxation time parameter and thermophoresis parameter whereas nanoparticle concentration is increased. Ali *et al.* [35, 36] deployed finite element techniques to study respectively cross diffusion and rotating body force effects in viscoelastic nanofluid transport with Cattaneo-Christov double diffusion. Khan *et al.* [37] addressed Williamson non-Newtonian nanofluid slip flow in permeable media with the Cattaneo–Christov double diffusion model. Muhammad [38] analyzed the Cattaneo–Christov double diffusive transport from a curved stretching sheet in non-Darcy porous medium. Further investigations under non-Fourier and non-Fickian formulations are reported in Refs. [39-41]. All these studies have confirmed the considerable deviation in transport characteristics computed with the non-Fourier and non-Fickian formulations.

In modern nanofluid mechanics, non–Newtonian characteristics are an important consideration and more accurately simulate the behaviour of these colloidal suspensions than conventional Newtonian models. This is particularly significant in materials processing where concentrations of nanoparticles can significantly modify the heat and mass behaviour, as noted by Pattniak *et al.* [42]. A diverse range of non-Newtonian nanofluid transport studies have been communicated in recent years where many different rheological formulations have been successfully utilized including micropolar nanofluids [43, 44], Jeffreys viscoelastic nanofluids [45], Casson viscoplastic nanofluids [46], Riner-Rivlin third grade viscoelastic nanofluids [47, 48], Eyring-Powell model [49], nonlinear radiative Oldroyd-B nanofluids [50], EMHD based second-grade nanofluids [51], micropolar nanofluids magnetized flow [52], Casson nanofluids [53], chemically reactive Burgers fluid [54], bioconvective viscous and couple-stress nanofluids [55, 56].

In the present study, motivated by simulating nano-polymer coating flows [57, 58], the non–Newtonian tangent hyperbolic nanofluid model is deployed in conjunction with the Buongiorno [59] nanoscale two-component model to analyze the *non-Newtonian nanofluid boundary layer flow from a stretching flat surface*. Thermal and species diffusion are characterized using the Cattaneo–Christov double diffusion theory. The effects of Brownian motion and thermophoresis are also included as are thermal absorption/generation. The inclusion of these

effects constitutes the novelty of the present study which generalizes previous works in Buongiorno nanofluid dynamics to address non-Fourier and non-Fickian physics and heat source/sink effects. The nonlinear dimensionless transformed ordinary differential boundary value problem has been solved with the exceptionally accurate, rapidly convergent Homotopy analysis method (HAM) [60]. Extensive graphical visualization is included of the effects of multiple emerging parameters on velocity, temperature and concentration profiles. Tabulated results for skin friction, Nusselt number and Sherwood number are also presented. The present work constitutes a novel contribution to the scientific literature.

2.   Mathematical Model for non-Newtonian nanofluid transport

The regime under investigation comprises the steady mixed convective boundary layer flow of an incompressible tangent hyperbolic nanofluid from a stretching surface. The surface is extended with non–linear velocity. A Cartesian coordinate system (*x-y*) is adopted in which the *x*-axis is aligned with the plane, while the *y*-axis is perpendicular to it, as depicted in Fig. 1. The Cattaneo–Christov double diffusion model is deployed. The effects of viscous dissipation are not considered due to the assumption of low velocity flow. Viscous dissipation greatly depends on the deformation in the fluid flow. Thus, viscous dissipation can be neglected in the case of small deformation in the fluid or low velocity flow. The conservation equations for mass, momentum and energy in the non-Newtonian, non-Fourier, non-Fickian boundary layer flow may be stated as follows by amalgamating the earlier models of given in [17]-[19] are:

$$\frac{\partial u}{\partial x} + \frac{\partial v}{\partial y} = 0, \tag{1}$$

$$\begin{cases} u\dfrac{\partial u}{\partial x} + v\dfrac{\partial v}{\partial y} = \upsilon(1-\lambda)\dfrac{\partial^2 u}{\partial y^2} + \sqrt{2}\upsilon\Gamma\lambda\left(\dfrac{\partial u}{\partial y}\right)\dfrac{\partial^2 u}{\partial y^2} - \\ + g\left\{\Lambda_1(T-T_\infty) + \Lambda_2(T-T_\infty)^2\right\} + g\left\{\Lambda_3(C-C_\infty) + \Lambda_4(C-C_\infty)^2\right\}, \end{cases} \tag{2}$$
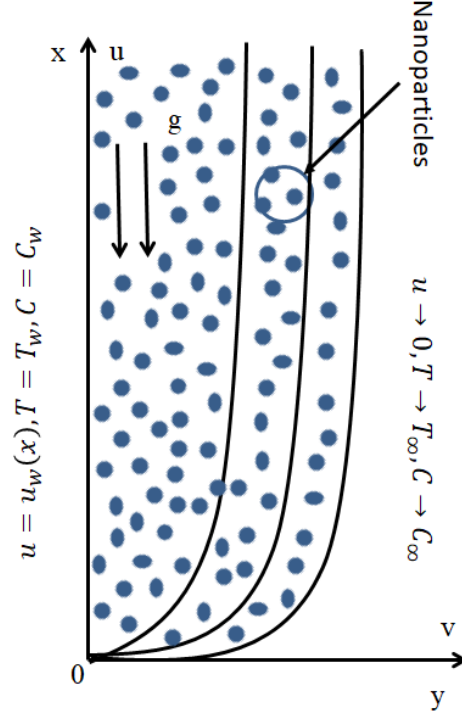
Fig. 1. Physical model

$$\left\{\begin{array}{l} u\dfrac{\partial T}{\partial x}+v\dfrac{\partial T}{\partial y}=\alpha\dfrac{\partial^2 T}{\partial y^2}-\lambda_t\left[\begin{array}{l}\dfrac{\partial T}{\partial x}\left(u\dfrac{\partial u}{\partial x}+v\dfrac{\partial u}{\partial y}\right)+\dfrac{\partial T}{\partial y}\left(u\dfrac{\partial v}{\partial x}+v\dfrac{\partial v}{\partial y}\right)\\[4mm] +2uv\dfrac{\partial^2 T}{\partial x\partial y}+u^2\dfrac{\partial^2 T}{\partial x^2}+v^2\dfrac{\partial^2 T}{\partial y^2}\end{array}\right]\\[10mm] +D_B\lambda_t\tau\left[u\dfrac{\partial^2 C}{\partial x\partial y}\dfrac{\partial T}{\partial y}+u\dfrac{\partial C}{\partial y}\dfrac{\partial^2 T}{\partial x\partial y}+v\dfrac{\partial^2 C}{\partial y^2}\dfrac{\partial T}{\partial y}+v\dfrac{\partial C}{\partial y}\dfrac{\partial^2 T}{\partial y^2}\right]\\[8mm] +2\lambda_t\tau\dfrac{D_T}{T_\infty}\left[u\dfrac{\partial T}{\partial y}\dfrac{\partial^2 T}{\partial x\partial y}+v\dfrac{\partial^2 T}{\partial y^2}\dfrac{\partial T}{\partial y}\right]+\dfrac{Q_0}{(\rho c)_f}(T-T_\infty)+\dfrac{Q_0}{(\rho c)_f}\lambda_t\left[u\dfrac{\partial T}{\partial x}+v\dfrac{\partial T}{\partial y}\right],\end{array}\right.$$

(3)

$$\begin{cases} u\dfrac{\partial C}{\partial x}+v\dfrac{\partial C}{\partial y}=D_B\dfrac{\partial^2 C}{\partial y^2}-\lambda_c\left[\begin{array}{c}\dfrac{\partial C}{\partial x}\left(u\dfrac{\partial u}{\partial x}+v\dfrac{\partial u}{\partial y}\right)+\dfrac{\partial C}{\partial y}\left(u\dfrac{\partial v}{\partial x}+v\dfrac{\partial v}{\partial y}\right)\\[3mm] +2uv\dfrac{\partial^2 C}{\partial x\partial y}+u^2\dfrac{\partial^2 C}{\partial x^2}+v^2\dfrac{\partial^2 C}{\partial y^2}\end{array}\right]\\[6mm] -\dfrac{D_T}{T_\infty}\lambda_c\left[u\dfrac{\partial^3 T}{\partial x\partial y^2}+v\dfrac{\partial^3 T}{\partial y^3}+\dfrac{\partial^2 T}{\partial y^2}\right],\end{cases} \tag{4}$$

The prescribed boundary conditions at the wall and in the free stream are:

$$u=u_w\left(x\right)=cx,\ v=0,\ T=T_w,\ C=C_w\ \text{at}\ y=0, \tag{5}$$

$$u\to 0,\ T\to T_\infty,\ C\to C_\infty\ \text{when}\ y\to\infty. \tag{6}$$

Here $\upsilon\left(=\dfrac{\mu}{\rho_f}\right)$ signifies the kinematic viscosity, ρ_f is liquid density, λ is material power-law index, g is gravitational acceleration, $\left(\Lambda_1,\Lambda_3\right)$ are linear (thermal, concentration) expansion coefficients, $\left(\Lambda_2,\Lambda_4\right)$ are nonlinear (thermal, concentration) expansion coefficients, $\alpha=\dfrac{k}{\left(\rho c\right)_f}$ is thermal diffusivity, μ is dynamic viscosity, $\tau=\dfrac{\left(\rho c\right)_p}{\left(\rho c\right)_f}$ is heat capacity ratio with $\left(\rho c\right)_f$ denoting liquid heat capacity, Γ is tangent-hyperbolic rheological material constant, $\left(\rho c\right)_p$ is nanoparticle heat capacity, Q_0 is coefficient of heat absorption/generation, $\left(D_T,D_B\right)$ designate (thermophoresis, Brownian) diffusion coefficients, $\left(T,C\right)$ are nanofluid (temperature, concentration), $u_w\left(x\right)$ is stretching velocity, k is thermal conductivity, c is stretching rate, $\left(\lambda_t,\ \lambda_c\right)$ are the relaxation times (non-Fourier thermal, non-Fickian solutal) $\left(T_\infty,C_\infty\right)$ represent ambient nanofluid (temperature, concentration) respectively and $\left(u,v\right)$ are velocity components in the $\left(x,y\right)$ directions respectively.

Introducing the following transformations:

$$\eta = y\sqrt{\frac{c}{\upsilon}}, u = cxf'(\eta), v = -\sqrt{c\upsilon}f(\eta),\ \theta(\eta) = \frac{T - T_\infty}{T_w - T_\infty},\ \phi(\eta) = \frac{C - C_\infty}{C_w - C_\infty}. \qquad (7)$$

Implementing Eqn. (7) in Eqns. (1)-(6), the mass conservation Eqn. (1) is automatically satisfied and Eqns. $(2) - (6)$ assume the dimensionless form:

$$(1 - \lambda)f''' - f'^2 + f\,f'' + \lambda We\,f''\,f''' + \delta\left[(1 + \beta_t\theta)\theta + N(1 + \beta_c\phi)\phi\right] = 0, \qquad (8)$$

$$\theta'' + \Pr\left(f\theta' + N_b\phi'\theta' + N_t\theta'^2 + S\theta + S\delta_1 f\theta'\right)$$
$$+ \Pr\delta_1\left(-ff'\theta' - f^2\theta'' - 2N_t f\theta'\theta'' - N_b f\theta'\phi'' - N_b f\theta''\phi'\right) = 0, \qquad (9)$$

$$\phi'' + Scf\phi' + \frac{N_t}{N_b}\theta'' + Sc\,\delta_2\left(-ff'\phi' - f^2\phi''\right) - \delta_2\frac{N_t}{N_b}f\theta'' = 0, \qquad (10)$$

$$f = 0,\ f' = 1,\ \theta = 1,\ \phi = 1 \text{ at } \eta \to 0, \qquad (11)$$

$$f' \to 0,\ \theta \to 0,\ \phi \to 0 \text{ as } \eta \to \infty. \qquad (12)$$

Here $(')$ signifies differentiation with respect to η, We is Weissenberg number, δ is mixed convection parameter, Gr_x is thermal Grashof number, N is the ratio of concentration to thermal buoyancy, Gr_x^* is the concentration Grashof number, (β_t, β_c) are nonlinear (thermal, concentration) convection variables, N_t is thermophoresis variable, $\Pr$ is Prandtl number, N_b is Brownian dynamics parameter, $S > 0$ corresponds to heat generation, $S < 0$ implies heat absorption, Sc is Schmidt number, Re_x is local Reynolds number and (δ_1, δ_2) are (thermal, solutal) relaxation times. These variables are defined as follows:

$$We = \frac{\sqrt{2}}{\sqrt{\upsilon}}\Gamma c^{\frac{3}{2}}x,\ \delta = \frac{Gr_x}{\mathrm{Re}_x^2},\ Gr_x = \frac{g\Lambda_1(T_w - T_\infty)x^3}{\upsilon^2},\ Gr_x^* = \frac{g\Lambda_3(C_f - C_\infty)x^3}{\upsilon^2},$$

$$\beta_t = \frac{\Lambda_2(T_f - T_\infty)}{\Lambda_1},\ \beta_c = \frac{\Lambda_4 C_\infty}{\Lambda_3},\ N = \frac{Gr_x^*}{Gr_x},\ \mathrm{Re}_x = \frac{xu_w}{\upsilon},\ N_t = \frac{\tau D_T(T_f - T_\infty)}{T_\infty\upsilon},$$

$$\Pr = \frac{\upsilon}{\alpha},\ N_b = \frac{\tau D_B(C_f - C_\infty)}{\upsilon},\ \delta_1 = \lambda_t c,\ \delta_2 = \lambda_c c,\ S = \frac{Q_0}{(\rho c)_f c},\ h = \frac{\upsilon_w}{\sqrt{c\upsilon}},$$

$$Sc = \frac{\upsilon}{D_B} \qquad (13)$$

The skin–friction coefficient is defined as:

$$C_{fx} = \frac{2\tau_w}{\rho u_w^2}, \; \tau_w = \mu \left[(1-\lambda)\frac{\partial u}{\partial y} + \lambda \frac{\Gamma}{\sqrt{2}} \left(\frac{\partial u}{\partial y}\right)^2 \right]_{y=0}, \tag{14}$$

The non–dimensional form of skin friction is:

$$C_{fx} \, \mathrm{Re}_x^{-\frac{1}{2}} = (1-\lambda)f''(0) + \frac{\lambda}{2} We \left(f''(0)\right)^2. \tag{15}$$

In present study, the Nusselt and Sherwood numbers are not computed because fluxes (heat and mass) for the case non-Fourier-Fick situation are not available in explicit form. However, the non-dimensional Nusselt and Sherwood numbers for Fourier-Fick situation are:

$$Nu_x \, \mathrm{Re}_x^{-\frac{1}{2}} = -\theta'(0),$$
$$Sh_x \, \mathrm{Re}_x^{-\frac{1}{2}} = -\phi'(0). \tag{16}$$

3.   Homotopy analysis method (HAM) Solutions

HAM [60] allows higher order power series approximations for differential equations and is implemented to solve the nonlinear ordinary differential boundary value problem defined by Eqns. (8)-(12). The initial guesses $\left(f_o(\eta), \theta_o(\eta), \phi_o(\eta)\right)$ and auxiliary linear operators $\left(L_f, L_\theta, L_\phi\right)$ are defined as:

$$f_0(\eta) = \left(1 - e^{-\eta}\right), \; \theta_0(\eta) = e^{-\eta}, \; \phi_0(\eta) = e^{-\eta}, \tag{17}$$

$$\begin{cases} L_f = f''' - f', \\ L_\theta = \theta'' - \theta, \\ L_\phi = \phi'' - \phi, \end{cases} \tag{18}$$

with

$$\begin{cases} L_f \left(C_1 + C_2 e^{\eta} + C_3 e^{-\eta}\right) = 0, \\ L_\theta \left(C_4 e^{\eta} + C_5 e^{-\eta}\right) = 0, \\ L_\phi \left(C_6 e^{\eta} + C_7 e^{-\eta}\right) = 0, \end{cases} \tag{19}$$

where $C_i (i = 1-7)$ indicate the arbitrary constants.

4. Convergence analysis of HAM

HAM convergence has been examined carefully. This involves the use of an auxiliary parameter h , which facilitates in adjusting the convergence area of velocity $f''(0)$, temperature $\theta'(0)$ and concentration $\phi'(0)$. The auxiliary parameter h therefore plays a vital role. In Figs 2-4 the h–curves for convergence have been presented. It is observed that approved values of h_f, h_θ and h_ϕ in Figs. 2, 3 and 4 are $-1.9 \le h_f \le -0.1$, $-1.5 \le h_\theta \le -0.2$ and $-1.5 \le h_\phi \le -0.1$. As can be seen, convergence of velocity $f''(0)$, temperature $\theta'(0)$ and concentration $\phi'(0)$ is completed at 20th order of approximation, which is then adopted for all subsequent computations (see **Table 1**). The skin friction ($C_{fx} \operatorname{Re}_x^{-\frac{1}{2}}$) results are compared with the work of Akbar et al. [61] with the intention to authenticate the precision of the obtained analytical outcomes, as exhibited in Table 2, which illustrates a decent agreement.
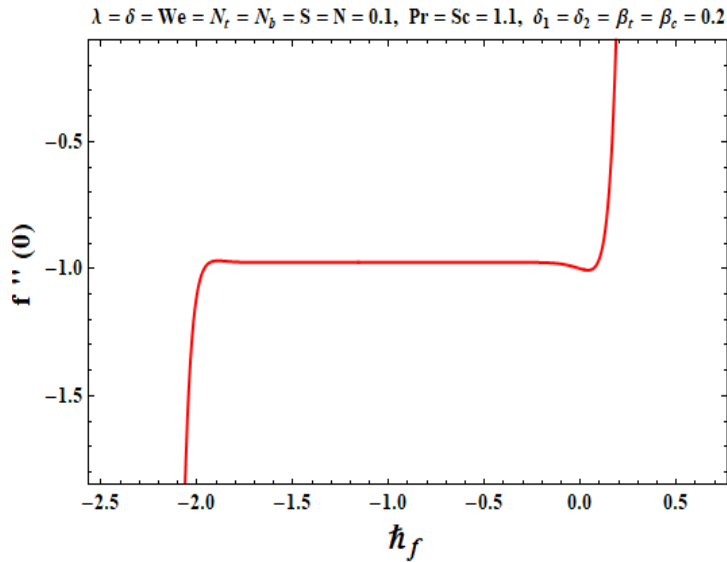

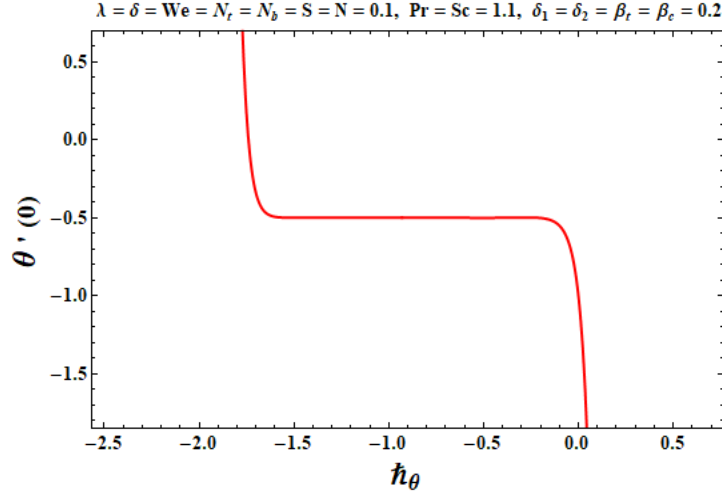$\lambda = \delta = \text{We} = N_t = N_b = S = N = 0.1, \ \text{Pr} = \text{Sc} = 1.1, \ \delta_1 = \delta_2 = \beta_t = \beta_c = 0.2$

Fig. 2. H– curve stimulus for $f''(0)$.

$\lambda = \delta = We = N_t = N_b = S = N = 0.1, \ Pr = Sc = 1.1, \ \delta_1 = \delta_2 = \beta_t = \beta_c = 0.2$

Fig. 3. H– curve stimulus for $\theta'(0)$.

$\lambda = \delta = We = N_t = N_b = S = N = 0.1, \ Pr = Sc = 1.1, \ \delta_1 = \delta_2 = \beta_t = \beta_c = 0.2$
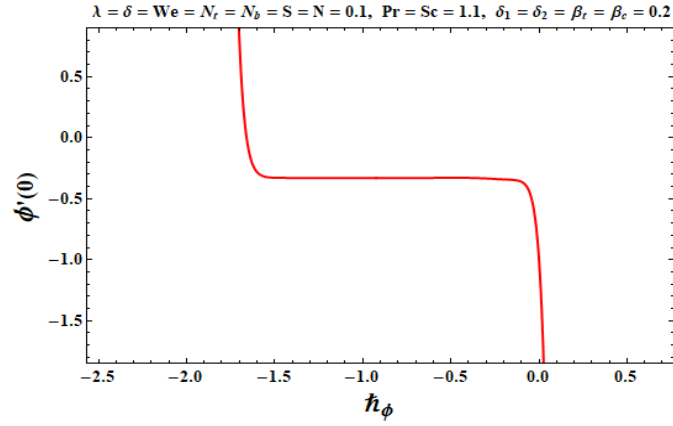

Fig. 4. H–curve stimulus for $\phi'(0)$.

Table 1. Convergence of HAM solutions when $We = \delta = \lambda = N_t = N_b = S = N = 0.1$, $Pr = Sc = 1.1$, $\delta_1 = \delta_2 = \beta_t = \beta_c = 0.2$.

Oder of approximations	$-f''(0)$	$-\theta'(0)$	$-\phi'(0)$
1	-0.9910	-0.5513	-0.1500
10	-0.9755	-0.4997	-0.3267
20	-0.9754	-0.4989	-0.3294
30	-0.9754	-0.4989	-0.3294
40	-0.9754	-0.4989	-0.3294
50	-0.9754	-0.4989	-0.3294

Table 2. Comparative outcomes of surface skin-friction ($C_{fx} \mathrm{Re}_x^{-\frac{1}{2}}$) when $\lambda = N = \beta_t = \beta_c = 0.0$.

λ	We	Akbar et al. [61]	Present study
0.0	0.0	1.00000	1.00000
0.1		0.94868	0.94868
0.2		0.89442	0.89443
0.0	0.3	1.00000	1.00000
0.1		0.94248	0.94248
0.2		0.88023	0.88023
0.0	0.5	1.00000	1.00000
0.1		0.93826	0.93826
0.2		0.87026	0.87026

5. HAM Results and Discussion

Figs. 5-21 depict the evolution in velocity, temperature, nanoparticle concentration and skin friction with selected parameters.
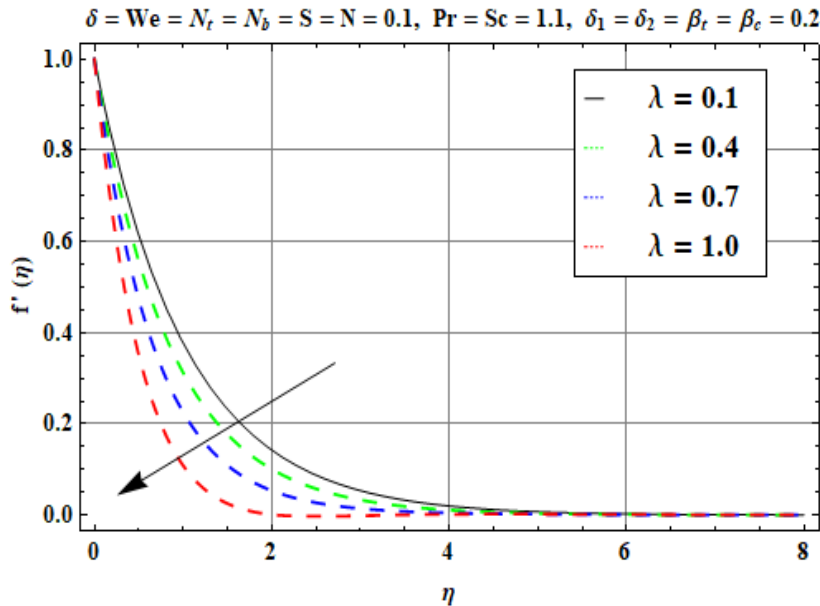

Fig. 5. $f'(\eta)$ against λ ($\delta = We = N_t = N_b = S = N = 0.1, \mathrm{Pr} = Sc = 1.1, \delta_1 = \delta_2 = \beta_t = \beta_c = 0.2$).
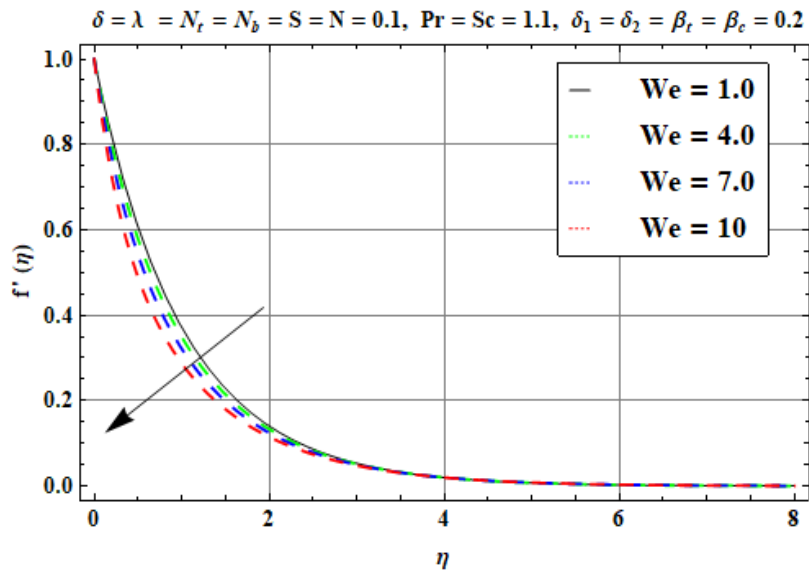
Fig. 6. $f'(\eta)$ against We ($\delta = \lambda = N_t = N_b = S = N = 0.1, \text{Pr} = Sc = 1.1, \delta_1 = \delta_2 = \beta_t = \beta_c = 0.2$)
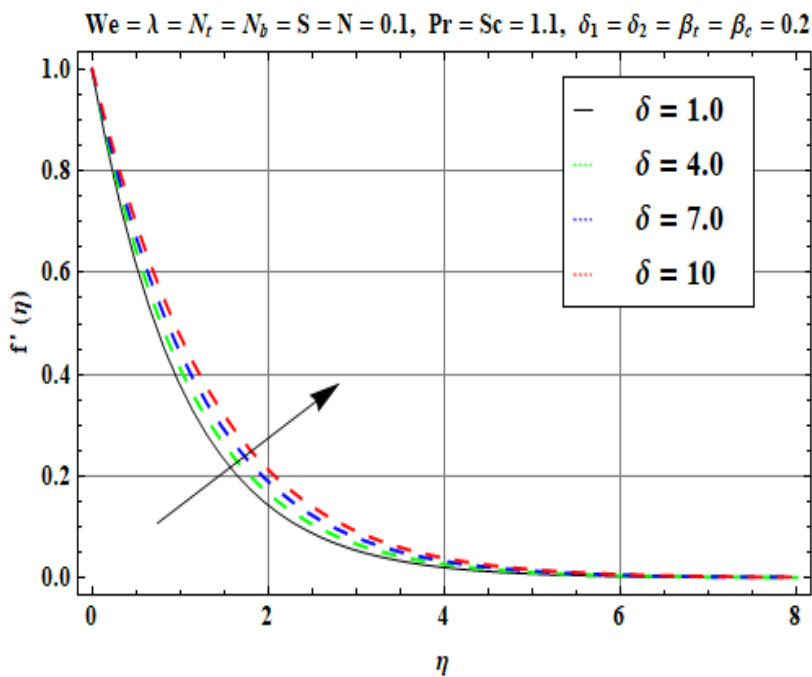

Fig. 7. $f'(\eta)$ against δ ($We = \lambda = N_t = N_b = S = N = 0.1, \text{Pr} = Sc = 1.1, \delta_1 = \delta_2 = \beta_t = \beta_c = 0.2$)

$$\lambda = \delta = We = N_t = N_b = N = 0.1, \ \mathbf{Pr} = \mathbf{Sc} = 1.1, \ \delta_1 = \delta_2 = \beta_t = \beta_c = 0.2$$
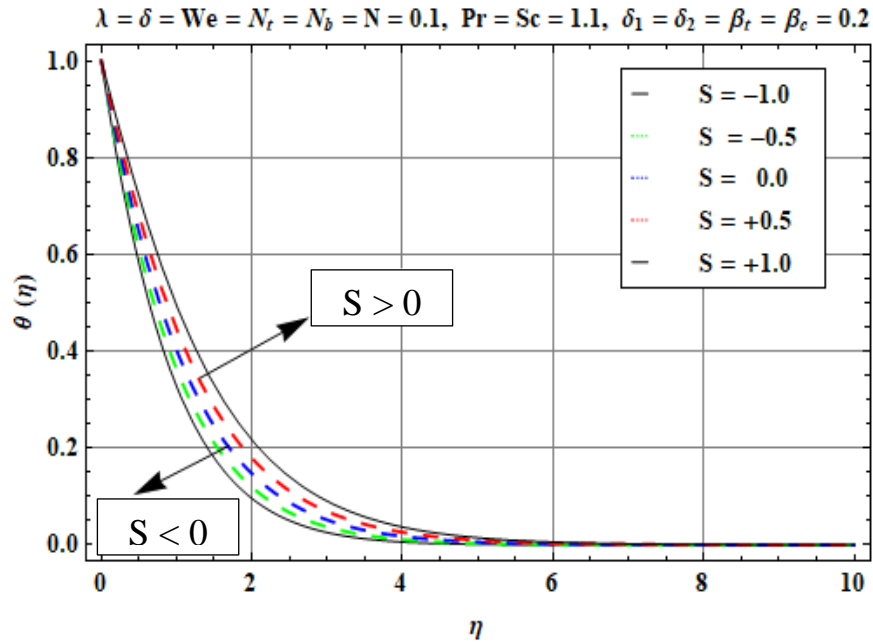
Fig. 8. $\theta(\eta)$ against S ($\lambda = \delta = We = N_t = 0.1, N_b = N = 0.1, \mathrm{Pr} = Sc = 1.1, \delta_1 = \delta_2 = \beta_t = \beta_c = 0.2$)
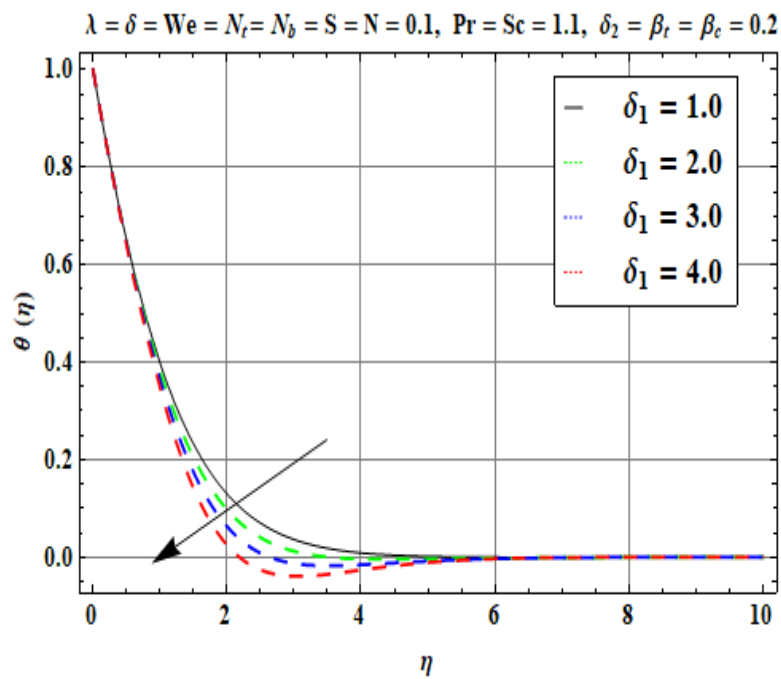

$$\lambda = \delta = We = N_t = N_b = S = N = 0.1, \ \mathbf{Pr} = \mathbf{Sc} = 1.1, \ \delta_2 = \beta_t = \beta_c = 0.2$$

Fig. 9. $\theta(\eta)$ against δ_1 ($\lambda = \delta = We = N_t = N_b = S = N = 0.1, \mathrm{Pr} = Sc = 1.1, \delta_2 = 0.2, \beta_t = \beta_c = 0.2$)
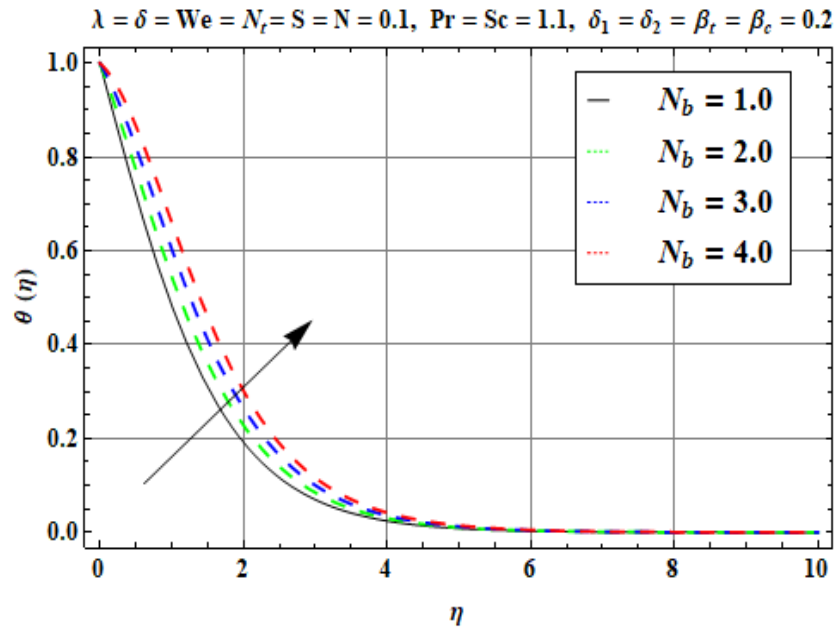
Fig. 10. $\theta(\eta)$ against N_b ($\lambda = \delta = We = N_t = 0.1, S = N = 0.1, \mathrm{Pr} = Sc = 1.1, \delta_1 = \delta_2 = \beta_t = \beta_c = 0.2$)

Fig. 11. $\theta(\eta)$ against N_t (with $\lambda = \delta = We = N_b = S = N = 0.1, \mathrm{Pr} = Sc = 1.1, \delta_1 = \delta_2 = \beta_t = \beta_c = 0.2$)

$\lambda = \delta = We = N_t = N_b = S = N = 0.1,\ Sc = 1.1,\ \delta_1 = \delta_2 = \beta_t = \beta_c = 0.2$

Fig. 12. $\theta(\eta)$ against Pr ($\lambda = \delta = We = N_t = N_b = S = N = 0.1, Sc = 1.1, \delta_1 = \delta_2 = \beta_t = \beta_c = 0.2$)
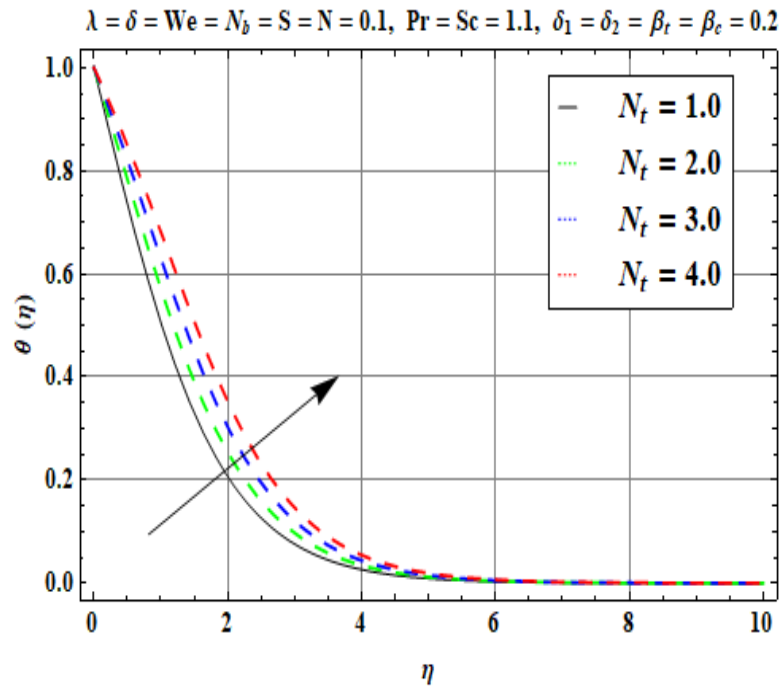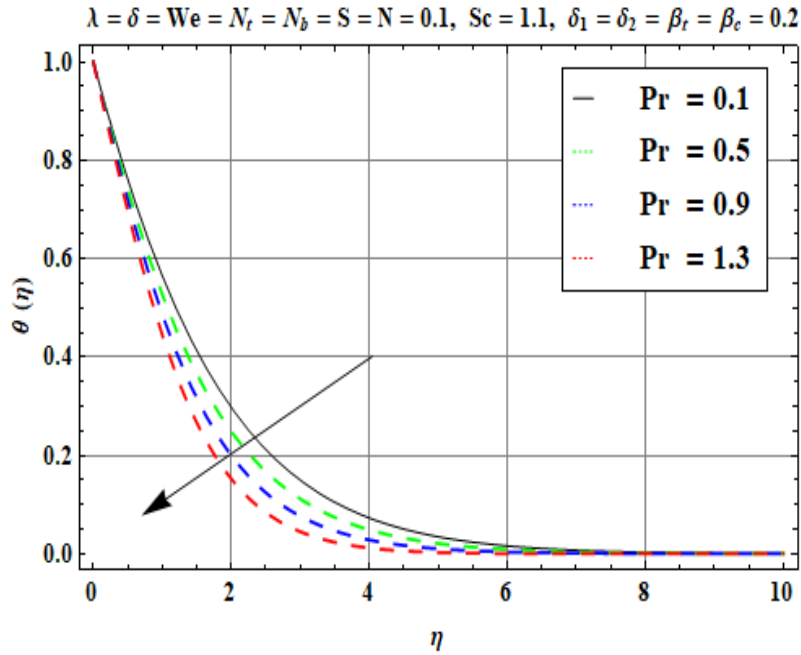
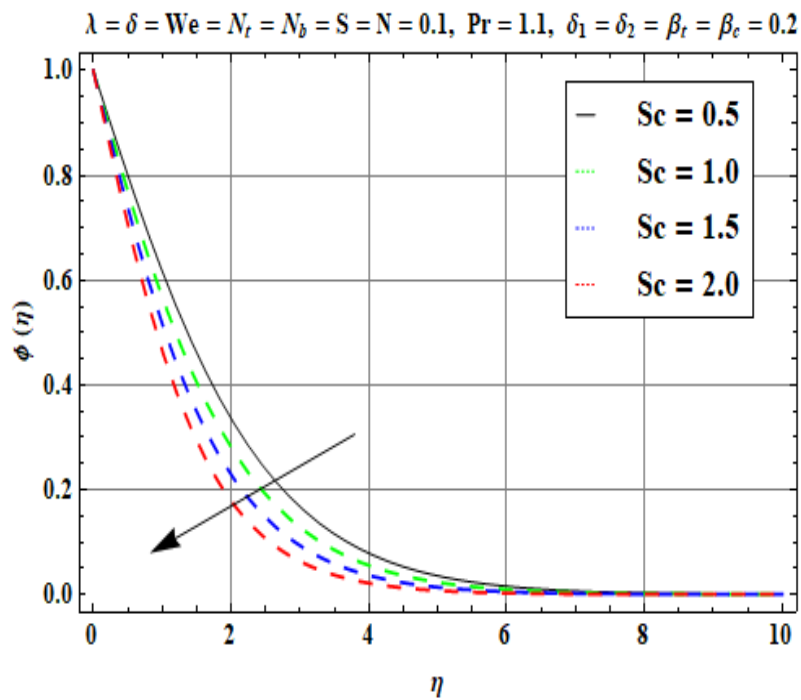$\lambda = \delta = We = N_t = N_b = S = N = 0.1,\ Pr = 1.1,\ \delta_1 = \delta_2 = \beta_t = \beta_c = 0.2$

Fig. 13. $\phi(\eta)$ against Sc ($\lambda = \delta = We = N_t = N_b = S = N = 0.1, Pr = 1.1, \delta_1 = \delta_2 = \beta_t = \beta_c = 0.2$)
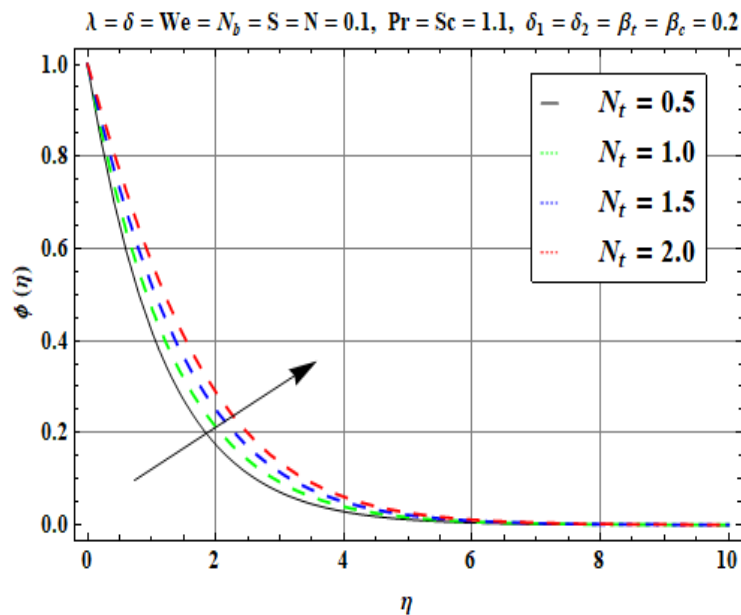
$$\lambda = \delta = We = N_b = S = N = 0.1, \ Pr = Sc = 1.1, \ \delta_1 = \delta_2 = \beta_t = \beta_c = 0.2$$

Fig. 14. $\phi(\eta)$ against N_t ($\lambda = \delta = We = N_b = S = N = 0.1$, $Pr = Sc = 1.1, \delta_1 = \delta_2 = \beta_t = \beta_c = 0.2$)

$$\lambda = \delta = We = N_t = S = N = 0.1, \ Pr = Sc = 1.1, \ \delta_1 = \delta_2 = \beta_t = \beta_c = 0.2$$
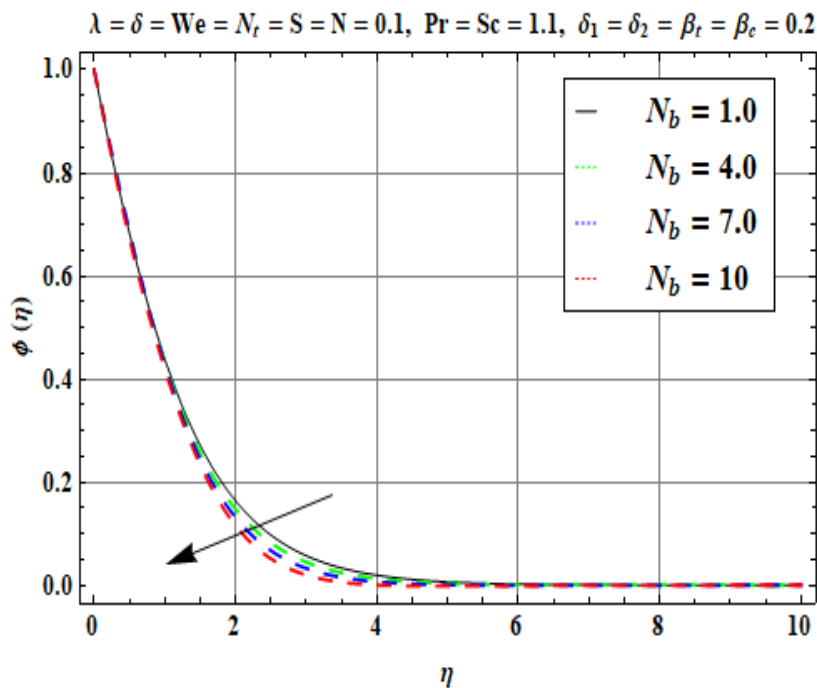

Fig. 15. $\phi(\eta)$ against N_b ($\lambda = \delta = We = N_t = S = N = 0.1$, $Pr = Sc = 1.1, \delta_1 = \delta_2 = \beta_t = \beta_c = 0.2$).

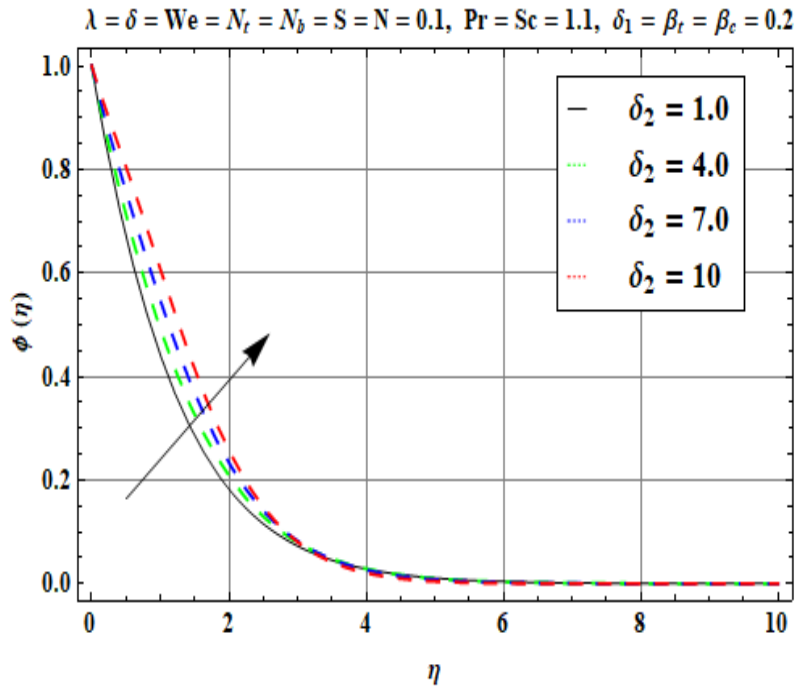$$\lambda = \delta = We = N_t = N_b = S = N = 0.1,\ Pr = Sc = 1.1,\ \delta_1 = \beta_t = \beta_c = 0.2$$

Fig. 16. $\phi(\eta)$ against δ_2 ($\lambda = \delta = We = N_t = N_b = S = N = 0.1, Pr = Sc = 1.1, \delta_1 = \beta_t = \beta_c = 0.2$)

$$\lambda = N_t = N_b = S = N = 0.1,\ Pr = Sc = 1.1,\ \delta_1 = \delta_2 = \beta_t = \beta_c = 0.2$$
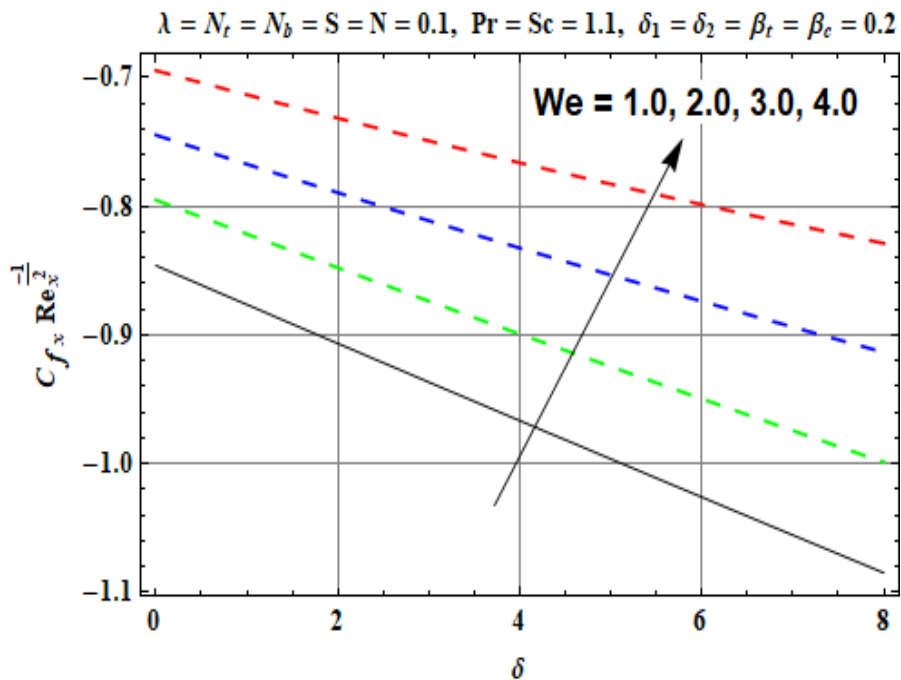
Fig. 17. $Cf_x \mathrm{Re}_x^{\frac{-1}{2}}$ against We.

$We = N_t = N_b = S = N = 0.1, \ Pr = Sc = 1.1, \ \delta_1 = \delta_2 = \beta_t = \beta_c = 0.2$

$\lambda = 0.1, 0.2, 0.3, 0.4$

Fig. 18. $Cf_x \, \mathrm{Re}_x^{\frac{-1}{2}}$ against λ.

$\lambda = N = N_t = N_b = S = We = 0.1, \ Pr = Sc = 1.1, \ \delta_1 = \delta_2 = \beta_c = 0.2$

$\beta_t = 1.0, \ 2.0, \ 3.0, \ 4.0$

Fig. 19. $Cf_x \, \mathrm{Re}_x^{\frac{-1}{2}}$ against β_t.

$We = N_t = N_b = S = \lambda = 0.1$, $Pr = Sc = 1.1$, $\delta_1 = \delta_2 = \beta_t = \beta_c = 0.2$

N = 1.0, 2.0, 3.0, 4.0
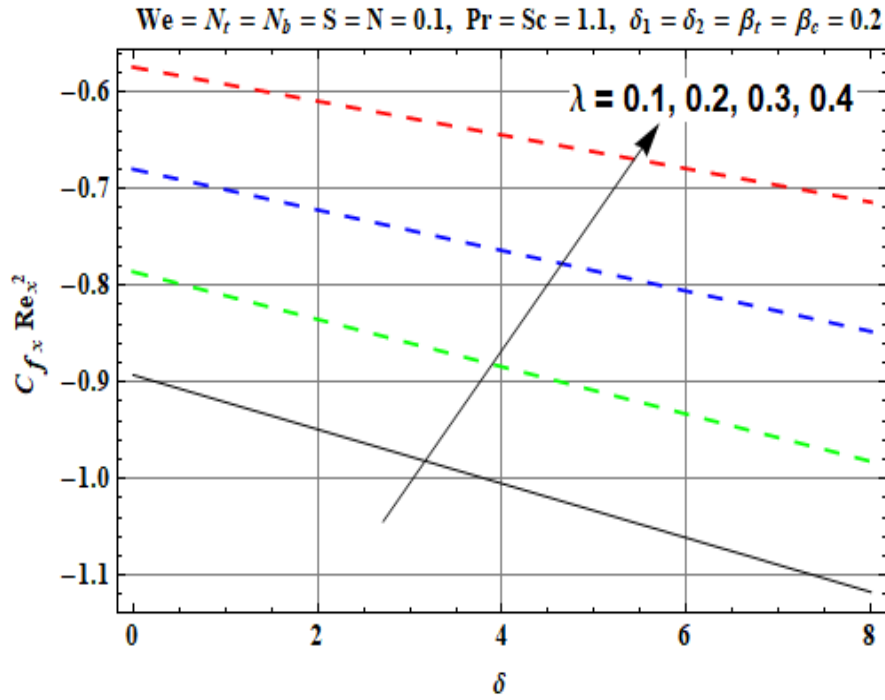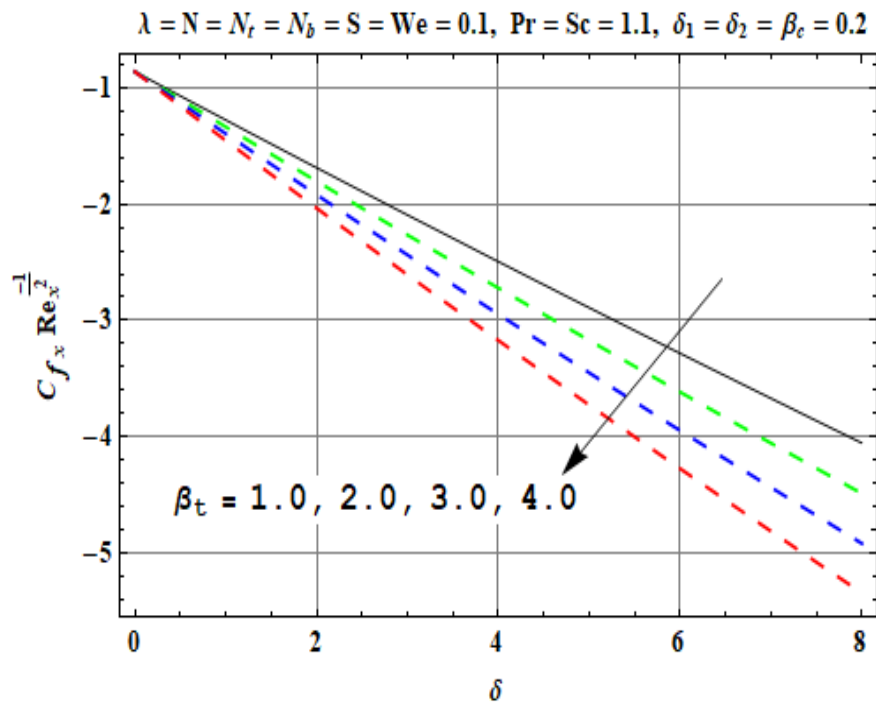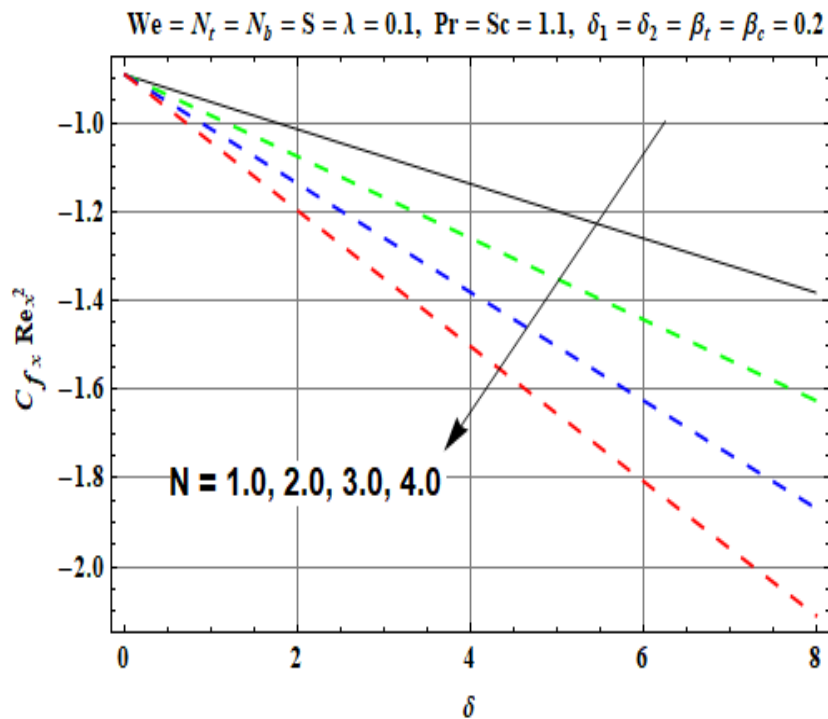
Fig. 20. $Cf_x \, Re_x^{\frac{-1}{2}}$ against N.

$\lambda = N = N_t = N_b = S = We = 0.1$, $Pr = Sc = 1.1$, $\delta_1 = \delta_2 = \beta_t = 0.2$

$\beta_c = 1.0$, 4.0, 7.0, 10.0
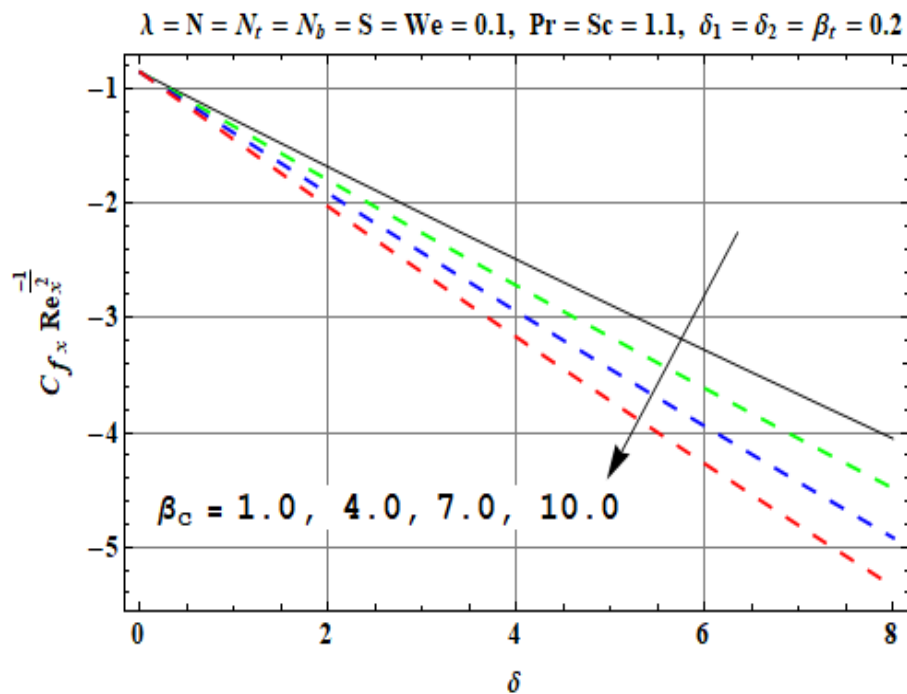
Fig. 21. $Cf_x \, Re_x^{\frac{-1}{2}}$ against β_c.

In **Figs. 5–7** Velocity distributions $\left(f' \right)$ are shown. The infinity boundary condition (edge of the boundary layer) is specified as $\eta = 8$ which achieves asymptotically smooth solutions in the free stream i.e. the range is evidently sufficient. The impact of non-Newtonian power–law index $\left(\lambda \right)$ on $f'(\eta)$ is plotted in Fig. 5, with the other parameters constrained as $\delta = We = N_t = N_b = S = N = 0.1, \mathrm{Pr} = Sc = 1.1, \delta_1 = \delta_2 = \beta_t = \beta_c = 0.2$. This data is accurate for certain nano-polymers and is extracted from [19]-[21]. With enhancement in $\left(\lambda = 0.1, 0.4, 0.7, 1.0 \right)$ there is a strong depletion in velocity $f'(\eta)$ i. e. the boundary layer flow is decelerated and there is an associated increase in momentum boundary layer thickness. The power-law index, λ, features in the modified shear terms in the momentum boundary layer Eqn. (8), viz, $(1 - \lambda)f''$ and $+ \lambda We f'' f'''$. As the value of this parameter increases, the behaviour becomes less pseudoplastic (shear-thinning) and viscosity increases. This decelerates the flow. The influence of Weissenberg number (We) on velocity $f'(\eta)$ is displayed in Fig. 6. The Weissenberg number $We = \frac{\sqrt{2}}{\sqrt{v}} \Gamma c^{\frac{3}{2}} x$ and is the ratio of the fluid relaxation time to a particular process time and also characterizes the relative contribution of elastic force to viscous force. It arises solely in the mixed derivative term, $+ \lambda We f'' f'''$ in the momentum boundary layer Eqn. (8). The other parameters are preset as $\delta = \lambda = N_t = N_b = S = N = 0.1, \mathrm{Pr} = Sc = 1.1, \delta_1 = \delta_2 = \beta_t = \beta_c = 0.2$. The velocity $f'(\eta)$ is also significantly reduced with increasing values of $(We = 1.0, 4.0, 7.0, 10.0)$. Momentum boundary layer thickness is therefore increased. It is also noteworthy that the Weissenberg number quantifies the degree of anisotropy or orientation generated by the deformation in the nanofluid, and is applicable for a constant stretch history, as studied in shearing flow (boundary layers). The influence of mixed convection variable $\left(\delta \right)$ on velocity $f'(\eta)$ is depicted in Fig. 7. There is a substantial enhancement in velocity $f'(\eta)$ with increment in $\left(\delta \right)$, with $We = \lambda = N_t = N_b = S = N = 0.1, \ \mathrm{Pr} = Sc = 1.1, \delta_1 = \delta_2 = \beta_t = \beta_c = 0.2$ fixed. The mixed convection parameter $\delta = \frac{Gr_x}{Re_x^2}$ and larger values correspond to stronger thermal buoyancy force relative to viscous hydrodynamic force. This accelerates the flow and results in a depletion in momentum boundary layer thickness. The strongest modification is computed at intermediate distances from the wall.

Figs. 8–12 visualize the impact of heat generation / absorption (S), non-Fourier thermal relaxation parameter (δ_1), thermophoresis (N_t), Brownian motion (N_b) and Prandtl number (Pr) on temperature $\theta(\eta)$. Fig. 8 illustrates the impact of (S) versus $\theta(\eta)$ with $\lambda = \delta = We = N_t = 0.1, N_b = N = 0.1, \text{Pr} = Sc = 1.1, \delta_1 = \delta_2 = \beta_t = \beta_c = 0.2$. The parameter, S, appears in two terms in the thermal boundary layer Eqn. (9), viz, $+S\theta$, $S\delta_1 f\theta'$ which are the classical Fourier and non-Fourier terms respectively, the latter featuring the thermal relaxation time, δ_1. With increment in positive S (heat generation) there is a strong accentuation in temperature $\theta(\eta)$ whereas the converse trend is computed for increment in negative S (i. e. heat absorption). This behaviour is similar to that computed with the classical Fourier model, although it is further amplified by the presence of thermal relaxation which significantly influences temperature distribution. Thermal boundary layer thickness is increased with heat generation (S >0) whereas it is reduced with heat absorption ($S<$) since the latter induces cooling in the boundary layer due to the removal of heat. Fig. 9 depicts the evolution in $\theta(\eta)$ with non-Fourier thermal relaxation parameter, (δ_1). This parameter in addition to being coupled to the heat generation/absorption term, , $S\delta_1 f\theta'$, also significantly modifies the other terms in the energy Eqn. (9) i.e. $Pr\,\delta_1\left(-ff'\theta' - f^2\theta'' - 2N_t f\theta'\theta'' - N_b f\theta'\phi'' - N_b f\theta''\phi'\right)$. As noted earlier, the non-Fourier parameter modifies the classical Fourier law of heat conduction achieving physically realistic *finite-speed* heat conduction and is a hyperbolic model rather than a parabolic model. As the thermal relaxation parameter is increased $(\delta_1 = 1.0, 2.0, 3.0, 4.0)$, with all other parameters fixed at $\lambda = \delta = We = N_t = N_b = S = N = 0.1, \text{Pr} = Sc = 1.1, \delta_2 = 0.2, \beta_t = \beta_c = 0.2$, there is a marked decay in temperatures, which is most pronounced at some distance from the wall. This decrement in temperatures is due to the delay in thermal diffusion associated with thermal relaxation and produces a reduced heating effect compared with the classical Fourier model. The nanofluid elements therefore takes longer to transport heat to neighboring fluid elements implying a slowing in thermal diffusion. Thermal boundary layer thickness is also reduced with increasing thermal relaxation. These observations are consistent with a number of other boundary layer nanofluid investigations including Hayat *et al.* [16] and Ibrahim [18]. The adoption of a non-

Fourier model therefore leads to significant modification in temperature distribution in the nanofluid.

Figs. 10 and 11 illustrate respectively the influence of nanoscale parameters i. e. Brownian motion (N_b) and thermophoresis (N_t) on temperature distribution $\theta(\eta)$ versus transverse coordinate (η). In Fig 10, $\lambda = \delta = We = N_t = 0.1$, $S = N = 0.1$, $Pr = Sc = 1.1$, $\delta_1 = \delta_2 = \beta_t = \beta_c = 0.2$ are fixed. The Brownian motion parameter simulates the random motion of nanoparticles in the nanofluid and arises in multiple terms in the thermal boundary layer i. e. energy conservation Eqn. (9), viz $Pr(N_b \phi' \theta')$ and $Pr\,\delta_1\left(-N_b f \theta' \phi'' - N_b f \theta'' \phi'\right)$. Furthermore, it arises in the nanoparticle concentration Eqn. (10), in the term, $-\delta_2 \frac{N_t}{N_b} f \theta''$. Brownian motion therefore exerts a prominent influence on the temperature and concentration distributions. Larger values of N_b imply smaller nanoparticle diameter in the Buongiorno model [59]. Therefore, as N_b increases, the number of ballistic collisions between nanoparticles in Brownian chaotic motion is amplified and this generates a heating effect which results in a temperature enhancement. Thermal boundary layer thickness is therefore strongly increased with N_b values. The temperature boost is sustained for some distance into the regime transverse to the wall. In Fig. 11, the temperature is also observed to be enhanced significantly with an increment in thermophoresis parameter, N_t, with $\lambda = \delta = We = N_b = S = N = 0.1$, $Pr = Sc = 1.1$, $\delta_1 = \delta_2 = \beta_t = \beta_c = 0.2$ prescribed. Thermophoretic parameter features also in multiple terms in the energy Eqn. (9), viz, $Pr\,(N_t \theta'^2)$ and $Pr\,\delta_1\left(-2N_t f \theta' \theta''\right)$ in addition to the coupling terms in the concentration Eqn. (10) i.e. terms, $+\frac{N_t}{N_b}\theta''$ and $-\delta_2 \frac{N_t}{N_b} f \theta''$. A substantial increase in temperature accompanies a rise in thermophoresis parameter $(N_t = 1.0, 2.0, 3.0, 4.0)$. Thermophoresis is the mobilization of nanoparticles under a temperature gradient which drives the nanoparticles to a cold region of the regime. This thermophoretic body force encourages thermal diffusion and heats the boundary layer also enhancing the thermal boundary layer thickness. The results computed concur with many other investigations including Hiremath *et al.* [47] and Ray *et al.* [49]. Overall, *both nanoscale effects* i. e. Brownian dynamics and thermophoresis favourably influence temperature distributions in the regime and confirm the excellent thermal enhancement properties of nanofluids.

Fig. 12 displays the response in $\theta(\eta)$ to a modification in Prandtl number, (Pr). For this graph, the values of the following parameters are preset as $\lambda = \delta = We = N_t = N_b = S = N =$

$0.1, Sc = 1.1, \delta_1 = \delta_2 = \beta_t = \beta_c = 0.2.$ An enhancement in $(\mathrm{Pr}=0.1, 0.5, 0.9, 1.3)$ induces a suppression in temperature $\theta(\eta)$ which is sustained at all values of transverse coordinate, η. Thermal diffusivity has an inverse relation with (Pr). Furthermore, Prandtl number is inversely proportional to the thermal conductivity of the nanofluid. Higher Prandtl number therefore implies a lower thermal conductivity which manifests in a cooling effect in the boundary layer and a concomitant depletion in the thermal boundary layer thickness.

Figs. 13–16 display the evolution in nanoparticle concentration distribution $\phi(\eta)$ for the effects of Schmidt number (Sc), thermophoresis variable (N_t), Brownian motion (N_b) and non-Fickian solutal relaxation (δ_2). Fig. 13 addresses the response of $\phi(\eta)$ to a variation in (Sc) and it is evident that there is a marked reduction in concentration magnitudes with greater Schmidt number $(Sc = 0.5, 1.0, 1.5, 2.0)$, with all other parameters fixed as $\lambda = \delta = We = N_t = N_b = S = N = 0.1$, $Pr = 1.1, \delta_1 = \delta_2 = \beta_t = \beta_c = 0.2$. Physically, Sc and mass diffusivity have an inverse relation to each other. Higher Schmidt number indicates lower mass (molecular) diffusivity, and this results in a depletion in nanoparticle concentration values throughout the boundary layer transverse to the wall. For $Sc > 1$ the molecular diffusivity exceeds the momentum diffusivity and vice versa for $Sc < 1$. The value of Schmidt number therefore has a dramatic effect on solutal (nanoparticle) diffusion in the regime. There will be an associated reduction also in nanoparticle concentration boundary layer thickness with greater Schmidt numbers. Fig. 14 shows that with increment in thermophoresis parameter $(N_t = 0.5, 1.0, 1.5, 2.0)$, with $\lambda = \delta = We = N_b = S = N = 0.1$, $Pr = Sc = 1.1, \delta_1 = \delta_2 = \beta_t = \beta_c = 0.2$, there is a substantial elevation in concentration $\phi(\eta)$ declining. As noted earlier, thermophoresis contributes via the terms, $+\frac{N_t}{N_b}\theta''$ and $-\delta_2 \frac{N_t}{N_b} f\theta''$ in the nanoparticle species diffusion Eqn. (10). The temperature gradient associated with thermophoretic body force also exacerbates nanoparticle diffusion and increases concentration boundary layer thickness. The influence of Brownian motion parameter (N_b) on nanoparticle concentration $\phi(\eta)$ is displayed in Fig. 15. Increasing values of Brownian motion parameter $(N_b = 1.0, 4.0, 7.0, 10.0)$ has the opposite effect to thermophoresis parameter, and strongly reduces the nanoparticle concentration $\phi(\eta)$. There is also an associated reduction in concentration boundary thickness.

The amplification in ballistic collisions between nanoparticles with greater *Nb* value (smaller diameter nanoparticles) energizes the regime i. e. generates heat. However, it inhibits nanoparticle diffusion through the regime since greater collisions prevent the migration of nanoparticles in the boundary layer. This manifests in a plummet in concentration values. This behaviour has been confirmed by Buongiorno [59] and is localized at some distance from the wall. Fig. 16 demonstrates that with elevation in non-Fickian solutal relaxation time parameter i.e. $(\delta_2 = 1.0, 4.0, 7.0, 10.0)$ with $\lambda = \delta = We = N_t = N_b = S = N = 0.1, \Pr = Sc = 1.1, \delta_1 = \beta_t = \beta_c = 0.2$, there is a significant boost in nanoparticle concentration $\phi(\eta)$. The parameter features in many terms in the nanoparticle concentration boundary layer Eqn. (10), viz, $+Sc\delta_2(-ff'\phi' - f^2\phi'')$ and $-\delta_2 \frac{N_t}{N_b} f\theta''$. The non-Fickian solutal relaxation therefore has the opposite effect on the nanoparticle species diffusion compared to the influence of non-Fourier thermal relaxation on the temperature distribution. The modification in concentration magnitudes is strongest near the wall. **Figs.17–21** display the influence of the tangent hyperbolic power–law index (λ), Weissenberg number (We), nonlinear (thermal, concentration) convection variables (β_t, β_c) and ratio of concentration to thermal buoyancy parameter (N) on skin friction coefficient $\left(Cf_x \operatorname{Re}_x^{\frac{-1}{2}} \right)$ versus mixed convection variable (δ). It is noted that, an enhancement in power–law index (λ) and Weissenberg number (We) produces a strong increase in the magnitude of $\left(Cf_x \operatorname{Re}_x^{\frac{-1}{2}} \right)$ as observed in Figs. 17 and 18, respectively. However, the profiles decay in a linear fashion in both graphs with an increment in the mixed convection variable (δ). However, there is a substantial depletion computed in the strong friction, $\left(Cf_x \operatorname{Re}_x^{\frac{-1}{2}} \right)$ with increment in (β_t, β_c, N) parameters, although once again there is a consistent depletion in skin friction with greater mixed convection variable (δ) and profiles all decay in a linear pattern. The parameters (β_t, β_c, N) all arise in the momentum boundary layer Eqn. (9) in the terms, $+\delta[(1 + \beta_t\theta)\theta + N(1 + \beta_c\phi)\phi]$. Greater concentration buoyancy force relative to thermal buoyancy force therefore decelerates the

boundary layer flow as does an increment in nonlinear convective thermal and concentration parameters.

6.   Conclusions

Inspired by simulating nano-polymeric coating flows in materials processing systems, a mathematical model has been developed for *non-Newtonian tangent hyperbolic nanofluid mixed convection boundary layer flow from a stretching flat surface with convective boundary conditions with heat absorption/generation and Cattaneo–Christov double diffusion (non-Fourier and non-Fickian) effects*. The Buongiorno nanoscale model has been deployed to analyze Brownian motion and thermophoretic body force effects. The nonlinear dimensionless transformed ordinary differential boundary value problem has been solved with the Homotopy analysis method (HAM). The convergence of HAM solutions has been studied in detail. The major findings of the simulations can be summarized as follows:

(i)   Velocity profile $f'(\eta)$ is enhanced with mixed convection parameter (δ) but suppressed with increment in Weissenberg number (We).

(ii)   With increasing Prandtl number (Pr) and non-Fourier thermal relaxation (δ_1) parameter there is a significant reduction in temperature $\theta(\eta)$ and thermal boundary layer thickness.

(iii)   Temperature $\theta(\eta)$ is enhanced with heat generation $(S>0)$ whereas it is depleted with heat absorption $(S<0)$.

(iv)   Temperature is elevated with an increase in Brownian motion parameter (N_b) and thermophoresis parameter (N_t).

(v)   Nanoparticle concentration $\phi(\eta)$ and concentration boundary layer thickness are enhanced substantially with an increase in non-Fickian solutal relaxation parameter (δ_2) whereas they are reduced with increasing Schmidt number (Sc) .

(vi)   Nanoparticle concentration $\phi(\eta)$ is enhanced with thermophoresis parameter (N_t) whereas it is reduced with Brownian motion parameter (N_b).

(vii)   Skin friction coefficient $\left(Cf_x \mathrm{Re}_x^{\frac{-1}{2}} \right)$ is markedly boosted with elevation in tangent hyperbolic power law index and Weissenberg number $(\lambda,\ We)$ whereas it is decreased with nonlinear thermal and concentration convection parameters and buoyancy ratio

(β_t, β_c, N) and also follows a linear decay with increasing values of mixed convection parameter (δ).

(viii)   HAM [60] has been shown to achieve excellent accuracy, stability and convergence in studying nonlinear multi-physical nano-polymeric coating flows.

The current study has examined the tangent hyperbolic non-Newtonian model for nanofluids. Future investigations may consider a variety of alternative non-Newtonian models including the Casson viscoplastic model [62], Reiner-Rivlin second grade viscoelastic model [63-65] or the Williamson model [66], which are all appropriate for simulating different aspects of nanofluid rheological behaviour.

Conflict of Interest

The authors declare that there is no conflict of interest.

References

1] Trujillo-de Santiago G, Rojas-de Gante C, García-Lara S, Ballescá-Estrada A, Alvarez MM (2014) Studying mixing in non-Newtonian blue maize flour suspensions using color analysis. *PLoS One* 9(11): e112954.

2] Maingonnat JF, Doublier JL, Lefebvre J, Delaplace G (2008) Power consumption of a double ribbon impeller with Newtonian and shear thinning fluids and during the gelation of an iota-carrageenan solution. *J. Food Eng*. 87: 82–90.

3] Syrjala S., Finite-element analysis of fully developed laminar flow of power-law non-Newtonian fluid in a rectangular duct, *Int. Comm. Heat Mass Transfer*, 22, 549-557 (1995).

4] D.A. Siginer, M.F. Letelier, Heat transfer asymptote in laminar flow of non-linear viscoelastic fluids in straight non-circular tubes, *Int. J. Engineering Science* 48(11) (2010) 1544 -1562.

5] N. S. Akbar, D. Tripathi, O. Anwar Bég, Z. H. Khan, MHD dissipative flow and heat transfer of Casson fluids due to metachronal wave propulsion of beating cilia with thermal and velocity slip effects under an oblique magnetic field, *Acta Astronautica,* 128, 1-12 (2016).

6] M. Izadi, Mikhail A.Sheremet, S.A.M.Mehryan, I.Pop, Hakan F.Öztop, N. Abu-Hamdeh, MHD thermo gravitational convection and thermal radiation of a micropolar nanoliquid in a porous chamber, *International Communications in Heat and Mass Transfer* 110, 2020.

7] D. Tripathi and O. Anwar Bég, Mathematical modeling of peristaltic propulsion of viscoplastic fluids, *Proc. IMechE- Part H; J. Engineering in Medicine,* 228 (1): 67-88 (2014).

8] V K Narla, Dharmendra Tripathi, O. Anwar Bég and A Kadir, Modelling transient magnetohydrodynamic peristaltic pumping of electroconductive viscoelastic fluids through a deformable curved channel, *Journal of Engineering Mathematics,* 111, 127–143(2018).

9] Ankita Dubey, B. Vas, O. Anwar Bég and R. S. R. Gorla, Finite element computation of magneto-hemodynamic flow and heat transfer in a bifurcated artery with saccular aneurysm using the Carreau-Yasuda biorheological model, *Microvascular Research, 138 (2021) 104221 (16 pages).*

10] Mohamed El Gendy, O. Anwar Bég, A. Kadir, M.N. Islam and D. Tripathi, Computational fluid dynamics simulation and visualization of Newtonian and non-Newtonian transport in a peristaltic micro-pump, *J. Mech. Med. Biology,* 21 (8) 2150058 (2021) (23 pages).

11] Ashmore, J., Shen, A. Q., Kavehpour, H. P., Stone, H. A., & McKinley, G. H. (2008). Coating flows of non-Newtonian fluids: Weakly and strongly elastic limits. *Journal of Engineering Mathematics*, *60*(1), 17-41.

12] C.J.Lawrence and W.Zhou, Spin coating of non-Newtonian fluids, *Journal of Non-Newtonian Fluid Mechanics,* 39, 137-187 (1991).

13] N. Ali, A. Zaman, O. Anwar Bég, T. Hayat, Mathematical model for isothermal wire-coating from a bath of Giesekus viscoelastic fluid, *Chem. Eng. Comm.* 203, 1336-1248 (2016).

14] M. Shamshuddin, U. S. Khan, O. Anwar Bég, T.A. Bég, Hall current, viscous and Joule heating effects on steady radiative 3-D magneto-power-law polymer dynamics from an exponentially stretching sheet with power-law slip velocity: a numerical study, *Thermal Science and Engineering Progress, 20* (2020) 100732. doi.org/10.1016/j.tsep.2020.100732 (13 pages)

15] B. Vasu, R.S.R. Gorla, P. V. S. N. Murthy and O. Anwar Bég, Entropy analysis on convective film flow of power-law fluid with nanoparticles along an inclined plate, *J. Applied Mechanics and Technical Physics, 60, 5, 1-15 (2019).*

16] Hayat, T., Khan, M. I., Waqas, M., & Alsaedi, A. (2017). Stagnation point flow of hyperbolic tangent fluid with Soret-Dufour effects. *Results in Physics*, *7*, 2711-2717.

17]Hussain, A., Malik, M. Y., Salahuddin, T., Rubab, A., & Khan, M. (2017). Effects of viscous dissipation on MHD tangent hyperbolic fluid over a nonlinear stretching sheet with convective boundary conditions. *Results in Physics*, *7*, 3502-3509.

18] Ibrahim, W. (2017). Magnetohydrodynamics (MHD) flow of a tangent hyperbolic fluid with nanoparticles past a stretching sheet with second order slip and convective boundary condition. *Results in Physics*, *7*, 3723-3731.

19] Khan, M. I., Qayyum, S., Hayat, T., Khan, M. I., Alsaedi, A., & Khan, T. A. (2018). Entropy generation in radiative motion of tangent hyperbolic nanofluid in presence of activation energy and nonlinear mixed convection. *Physics Letters A*, *382*(31), 2017-2026.

20] Atif, S. M., Hussain, S., & Sagheer, M. (2019). Heat and mass transfer analysis of time-dependent tangent hyperbolic nanofluid flow past a wedge. *Physics Letters A*, *383*(11), 1187-1198.

21] Kebede, T., Haile, E., Awgichew, G., & Walelign, T. (2020). Heat and mass transfer analysis in unsteady flow of tangent hyperbolic nanofluid over a moving wedge with buoyancy and dissipation effects. *Heliyon*, *6*(4), e03776.

22] Awais, M., Kumam, P., Ali, A., Shah, Z., & Alrabaiah, H. (2021). Impact of activation energy on hyperbolic tangent nanofluid with mixed convection rheology and entropy optimization. *Alexandria Engineering Journal*, *60*(1), 1123-1135.

23] Ramzan, M., Gul, H., Kadry, S., & Chu, Y. M. (2021). Role of bioconvection in a three dimensional tangent hyperbolic partially ionized magnetized nanofluid flow with Cattaneo-Christov heat flux and activation energy. *International Communications in Heat and Mass Transfer*, *120*, 104994.

24] Shafiq, A., Sindhu, T. N., & Khalique, C. M. (2020). Numerical investigation and sensitivity analysis on bioconvective tangent hyperbolic nanofluid flow towards stretching surface by response surface methodology. *Alexandria Engineering Journal*, *59*(6), 4533-4548.

25] Metri, P. G., Metri, P. G., Abel, S., & Silvestrov, S. (2016). Heat transfer in MHD mixed convection viscoelastic fluid flow over a stretching sheet embedded in a porous medium with viscous dissipation and non-uniform heat source/sink. *Procedia Engineering*, *157*, 309-316.

26] Çolak, E., Öztop, H. F., & Ekici, Ö. (2020). MHD mixed convection in a chamfered lid-driven cavity with partial heating. *International Journal of Heat and Mass Transfer*, *156*, 119901.

27] Bhukta, D., Dash, G. C., Mishra, S. R., & Baag, S. (2017). Dissipation effect on MHD mixed convection flow over a stretching sheet through porous medium with non-uniform heat source/sink. *Ain Shams Engineering Journal*, *8*(3), 353-361.

28] Cattaneo, C. (1948). Sulla conduzione del calore. *Atti Sem. Mat. Fis. Univ. Modena*, *3*, 83-101.

29] Christov, C. I. (2009). On frame indifferent formulation of the Maxwell–Cattaneo model of finite-speed heat conduction. *Mechanics Research Communications*, *36*(4), 481-486.

30] Straughan, B. (2010). Thermal convection with the Cattaneo–Christov model. *International Journal of Heat and Mass Transfer*, *53*(1-3), 95-98.

31] Hayat, T., Qayyum, S., Shehzad, S. A., & Alsaedi, A. (2017). Chemical reaction and heat

generation/absorption aspects in flow of Walters-B nanofluid with Cattaneo-Christov double-diffusion. *Results in Physics*, *7*, 4145-4152.

32] Zhang, Y., Yuan, B., Bai, Y., Cao, Y., & Shen, Y. (2018). Unsteady Cattaneo-Christov double diffusion of Oldroyd-B fluid thin film with relaxation-retardation viscous dissipation and relaxation chemical reaction. *Powder Technology*, *338*, 975-982.

33] Ahmad, I., Faisal, M., & Javed, T. (2019). Bi-directional stretched nanofluid flow with Cattaneo-Christov double diffusion. *Results in Physics*, *15*, 102581.

34] Ijaz, M., & Ayub, M. (2019). Activation energy and dual stratification effects for Walter-B fluid flow in view of Cattaneo-Christov double diffusion. *Heliyon*, 5(6), e01815.

35] Ali, B., Hussain, S., Nie, Y., Hussein, A. K., & Habib, D. (2021). Finite element investigation of Dufour and Soret impacts on MHD rotating flow of Oldroyd-B nanofluid over a stretching sheet with double diffusion Cattaneo Christov heat flux model. *Powder Technology*, *377*, 439-452.

36] Ali, B., Nie, Y., Hussain, S., Manan, A., & Sadiq, M. T. (2020). Unsteady magneto-hydrodynamic transport of rotating Maxwell nanofluid flow on a stretching sheet with Cattaneo–Christov double diffusion and activation energy. *Thermal Science and Engineering Progress*, *20*, 100720.

37] Khan, M. I., Alzahrani, F., Hobiny, A., & Ali, Z. (2020). Modeling of Cattaneo-Christov double diffusions (CCDD) in Williamson nanomaterial slip flow subject to porous medium. *Journal of Materials Research and Technology*, *9*(3), 6172-6177.

38] Muhammad, T., Rafique, K., Asma, M., & Alghamdi, M. (2020). Darcy–Forchheimer flow over an exponentially stretching curved surface with Cattaneo–Christov double diffusion. *Physica A: Statistical Mechanics and its Applications*, *556*, 123968.

39] K. Gangadhar, K. R. Venkata, O. D. Makinde and B. R. Kumar, MHD flow of a Carreau fluid past a stretching cylinder with Cattaneo-Christov heat flux using spectral relaxation method, *Defect and Diffusion Forum*, 387 (2018) 91-105.

40] B. Mahanthesh, O. D. Makinde, B. J. Gireesha, K. L. Krupalakshmi and I. L. Animasaun, Two-phase flow of dusty Casson fluid with Cattaneo-Christov heat flux and heat source past a cone, wedge and plate, *Defect and Diffusion Forum*, 387 (2018) 625-639.

41] K. V. Ramana, K. Gangadhar, T. Kannan and A. J. Chamkha, Cattaneo–Christov heat flux theory on transverse MHD Oldroyd-B liquid over nonlinear stretched flow, *Journal of Thermal Analysis and Calorimetry* 147 (2022) 2749–2759.

42] P.K. Pattnaik, S. R. Mishra, O. Anwar Bég, Umar F. Khan and J.C. Umavathi, Axisymmetric radiative titanium dioxide magnetic nanofluid flow on a stretching cylinder with homogeneous/heterogeneous reactions in Darcy-Forchheimer porous media: *intelligent*

nanocoating simulation, Materials Science and Engineering B (2021). *doi.org/10.1016/j.mseb.2021.115589* (26 pages)

43] J.C. Umavathi and O. Anwar Bég, Simulation of the onset of convection in porous medium layer saturated by a couple stress nanofluid, *Microfluidics and Nanofluidics (2021). 25:53* *https://doi.org/10.1007/s10404-021-02448-5 (20 pages).*

44] P. K. Pattnaik, M. M. Bhatti, S. R. Mishra, Munawwar Ali Abbas and O. Anwar Bég, Mixed convective-radiative magnetized micropolar nanofluid flow over a stretching surface in porous media with double stratification and chemical reaction effects: ADM-Padé computation, *J. Mathematics* (2022). Volume 2022, Article ID 9888379 (19 pages). *https://doi.org/10.1155/2022/9888379*

45] Dharmendra Tripathi, J. Prakash, O. Anwar Bég and R. Kumar, Thermal analysis of $\gamma Al_2O_3/H_2O$ and $\gamma Al_2O_3/C_2H_6O_2$ elastico-viscous nanofluid flow driven by peristaltic wave propagation with electroosmotic and magnetohydrodynamic effects: applications in nanotechnology energy systems, *Book chapter, "Energy Systems and Nanotechnology", "Advances in Sustainability Science and Technology" Book Series, Springer-Nature, Singapore, (2021). doi.org/10.1007/978-981-16-1256-5_13, pp. 1-37.*

46] J. Prakash, Dharmendra Tripathi, O. Anwar Bég, A.K. Tiwari and R. Kumar, Thermoelectro kinetic rotating non-Newtonian hybrid nanofluid flow from an accelerating vertical surface, *Heat Transfer* (2021). DOI: 10.1002/htj.22373 (32 pages)

47] Ashwini Hiremath, G. Janardhana Reddy, O. Anwar Bég and H. Holla, Numerical investigation on transient third-grade magnetized nanofluid flow and radiative convection heat transfer from a stationary/moving cylinder: Nanomaterial and nanoparticle shape effects, *Waves in Random and Complex Media (2022). https://doi.org/10.1080/17455030.2021.2024300 (30 pages)*

48] M. K. Nayak, A. K. A. Hakeem and O.D. Makinde, Influence of Catteneo-Christov heat flux model on mixed convection flow of third grade nanofluid over an inclined stretched Riga plate, *Defect and Diffusion Forum* 387 (2018) 121-134.

49] Atul Kumar Ray, B. Vasu, P. V. S. N. Murthy, O. Anwar Bég, R.S.R. Gorla and B. Kumar, Convective flow of non-homogeneous rheological nanofluids with non-Fourier thermal relaxation -application in polymer coating, *Arabian J. Science Engineering* (2021). https://doi.org/10.1007/s13369-021-06467-w (18 pages)

50] K. Gangadhar, M. A. Kumari, M. V. S. Rao and A. J. Chamkha, Oldroyd-B nanoliquid flow through a triple stratified medium submerged with gyrotactic bioconvection and nonlinear radiations, *Arabian Journal for Science and Engineering* (2021). https://link.springer.com/content/pdf/10.1007/s13369-021-06412-x.pdf

51] K. Gangadhar, M. A. Kumari and A. J. Chamkha, EMHD flow of radiative second grade nanofluid over a Riga plate due to convective heating: revised Buongiorno's nanofluid model,

Arabian Journal for Science and Engineering (2021). https://link.springer.com/article/10.1007/s13369-021-06092-7

52] K. Gangadhar, T. Kannan and P. Jayalakshmi, Magnetohydrodynamic micropolar nanofluid past a permeable stretching/shrinking sheet with Newtonian heating, *Journal of the Brazilian Society of Mechanical Sciences and Engineering* 39 (2017) 4379–4391.

53] O. D. Makinde, V. Nagendramma, C. S. K. Raju and A. Leelarathnam, Effects of Cattaneo-Christov heat flux on Casson nanofluid flow past a stretching cylinder, *Defect and Diffusion Forum*, 378 (2017) 28-38.

54] K. Gangadhar, M. A. Kumari, M. V. S. Rao, K. Alnefaie, I. Khan and M. Andualem, Magnetization for Burgers' fluid subject to convective heating and heterogeneous-homogeneous reactions, *Computational Mathematics and Numerical Analysis* (2022). https://doi.org/10.1155/2022/2747676

55] K. Gangadhar, P. M. Seshakumari, M. V. S. Rao and A. J. Chamkha, Biconvective transport of magnetized couple stress fluid over a radiative paraboloid of revolution, *Proceedings of the Institution of Mechanical Engineers, Part E: Journal of Process Mechanical Engineering* (2022). https://doi.org/10.1177/09544089211072715

56] K. Gangadhar, K. B. Lakshmi, T. Kannan and A. J. Chamkha, Stefan blowing on chemically reactive nano-fluid flow containing gyrotactic microorganisms with leading edge accretion (or) ablation and thermal radiation, *Indian Journal of Physics* (2022). DOI: 10.1007/s12648-021-02179-x

57] Tadmor, Z, Gogos, CG. *Principles of Polymer Processing*. Hoboken, NJ: John Wiley Sons, 2006.

58] M.F. Fakoya and S.N. Shah, Rheological properties of surfactant-based and polymeric nano-fluids, *SPE/ICoTA Coiled Tubing & Well Intervention Conference & Exhibition*, The Woodlands, Texas, USA, March 2013.

59] J. Buongiorno, Convective transport in nanofluids, *ASME J. Heat Transfer*, 128, 240-25 (2006).

60] S.J. Liao, *Homotopy Analysis Method in Nonlinear Differential Equations*, Berlin & Beijing: Springer & Higher Education Press (2012).

59] M. Turkyilmazoglu, Equivalence of ratio and residual approaches in the homotopy analysis method and some applications in nonlinear science and engineering, *Computer Modeling in Engineering & Sciences*, *Vol.120, No.1, 2019, pp.63-81, doi:10.32604/cmes.2019.06858*

60] M. Turkyilmazoglu, Nonlinear problems via a convergence accelerated decomposition method of Adomian, *Computer Modeling in Engineering & Sciences*, (2021). DOI: 10.32604/CMES.2021.012595.

61] N. S. Akbar, S. Nadeem, R. U. Haq and Z. H. Khan, Numerical solutions of Magnetohydrodynamic boundary layer flow of tangent hyperbolic fluid towards a stretching sheet, *Indian journal of Physics*, 87, 1121-1124, (2013).

[62] Ganesh, N.V., et al., 2022. Buoyancy-driven convection of MWCNT-Casson nanofluid in a wavy enclosure with a circular barrier and parallel hot/cold fins. *Alexandria Engineering Journal*, 61(4), pp.3249-3264.

[63] Ganesh, N.V., et al., 2021. Buoyancy driven second grade nano boundary layers over a catalytic surface with reaction rate, heat of reaction and activation energy at boundary. *Case Studies in Thermal Engineering,* 28, p.101346.

[64] Kalaivanan, R., et al., 2021. Buoyancy driven flow of a second grade nanofluid flow taking into account the Arrhenius activation energy and elastic deformation: models and numerical results. *Fluid Dynam. Mater. Process*, 17(2), pp.319-332.

[65] Kalaivanan, R., et al., 2020. An investigation on Arrhenius activation energy of second grade nanofluid flow with active and passive control of nanomaterials. *Case Studies in Thermal Engineering,* 22, p.100774.

[66] Dadheech, A., et al., 2022. Second law analysis for MHD slip flow for Williamson fluid over a vertical plate with Cattaneo-Christov heat flux. *Case Studies in Thermal Engineering*, p.101931.